Cellular Microbiology (2016) **18**(5), 748–760
doi:10.1111/cmi.12548
First published online 27 December 2015

Lysosome biogenesis/scattering increases host cell susceptibility to invasion by *Trypanosoma cruzi* metacyclic forms and resistance to tissue culture trypomastigotes

Cristian Cortez, Fernando Real[†] and Nobuko Yoshida[*]
Departamento de Microbiologia, Imunologia e Parasitologia, Escola Paulista de Medicina, Universidade Federal de São Paulo, R. Pedro de Toledo, 669-6° andar04039-032 São Paulo, SP, Brazil.

Summary

A fundamental question to be clarified concerning the host cell invasion by *Trypanosoma cruzi* is whether the insect-borne and mammalian-stage parasites use similar mechanisms for invasion. To address that question, we analysed the cell invasion capacity of metacyclic trypomastigotes (MT) and tissue culture trypomastigotes (TCT) under diverse conditions. Incubation of parasites for 1 h with HeLa cells in nutrient-deprived medium, a condition that triggered lysosome biogenesis and scattering, increased MT invasion and reduced TCT entry into cells. Sucrose-induced lysosome biogenesis increased HeLa cell susceptibility to MT and resistance to TCT. Treatment of cells with rapamycin, which inhibits mammalian target of rapamycin (mTOR), induced perinuclear lysosome accumulation and reduced MT invasion while augmenting TCT invasion. Metacylic trypomastigotes, but not TCT, induced mTOR dephosphorylation and the nuclear translocation of transcription factor EB (TFEB), a mTOR-associated lysosome biogenesis regulator. Lysosome biogenesis/scattering was stimulated upon HeLa cell interaction with MT but not with TCT. Recently, internalized MT, but not TCT, were surrounded by colocalized lysosome marker LAMP2 and mTOR. The recombinant gp82 protein, the MT-specific surface molecule that mediates invasion, induced mTOR dephosphorylation, nuclear TFEB translocation and lysosome biogenesis/scattering. Taken together, our data clearly indicate that MT invasion is mainly lysosome-dependent, whereas TCT entry is predominantly lysosome-independent.

Received 31 August, 2015; revised 8 October, 2015; accepted 11 November, 2015. *For correspondence. E-mail nyoshida@unifesp.br; Tel. 55 11 55764987.
Present addresses:[†]Department d'Infection, Immunité et Inflammation, Institut Cochin, INSERM U1016, Paris, France.

Introduction

For successful infection of mammalian hosts, intracellular pathogens have evolved diverse strategies to invade host cells, as well to survive and replicate intracellularly. After invasion, which may be mainly pathogen-driven or dependent on host cell processes, many pathogens are initially lodged in endocytic or phagocytic vesicles, which ultimately fuse with lysosomes, the organelles full of degradative enzymes. Some pathogenic bacteria can survive in a compartment derived from fusion of the vacuole with lysosomes, because of their resistance to lysosomal pH and enzymes (Voth and Heinzen, 2007). Other bacteria escape from the phagosome before lysosome fusion, reaching the host cell cytosol where they replicate (Goebel and Kuhn, 2000), or delay phagolysosome maturation (Deretic *et al.,* 2006).

Trypanosoma cruzi, the protozoan parasite that causes Chagas disease and is transmitted by triatomine insects, can invade different mammalian cell types. Following cell invasion by insect-derived metacyclic trypomastigotes, the parasites replicate as amastigotes that subsequently differentiate into trypomastigotes, which are released into circulation and disseminate the infection to diverse organs and tissues, where they invade cells and go through additional rounds of intracellular multiplication. To elucidate the mechanisms of host cell invasion by *T. cruzi*, metacyclic trypomastigote (MT) generated *in vitro* and tissue culture-derived trypomastigote (TCT) have been used as the equivalents of insect-borne and bloodstream parasite forms respectively. About two decades ago, it was reported that TCT invasion relied on exocytosis of host cell lysosomes recruited to the plasma membrane at

the site of parasite attachment in a Ca^{2+}-dependent manner, for the parasitophorous vacuole biogenesis (Tardieux *et al.,* 1992; Rodríguez *et al.,* 1995; Rodriguez *et al.,* 1996). Then, an alternative lysosome-independent model of TCT invasion was proposed 10 years ago (Burleigh, 2005), based on the findings that at early time points of infection, fewer parasites relative to total intracellular parasites were lysosome-associated, as opposed to about 50% of parasites associated with host cell plasma membrane markers and another 20% with early endosome markers (Woolsey *et al.,* 2003; Woolsey and Burleigh, 2004). As concerns MT, recent studies have shown that invasion of this parasite form is associated with exocytosis of lysosomes, which are mobilized from the perinuclear area to the cell periphery (Martins *et al.,* 2011). MT invasion increased when the parasites were incubated with host cells in nutrient-deprived medium, a condition that induced lysosome exocytosis (Martins *et al.,* 2011; Maeda *et al.,* 2012). If TCT invasion is in fact mainly lysosome-independent (Burleigh, 2005), this would imply that MT and TCT use diverse strategies to enter target cells. An indication that this may be the case was the finding that rapamycin, the inhibitor of the mammalian target of rapamycin (mTOR) inhibited MT invasion (Martins *et al.,* 2011) and stimulated TCT entry into host cells (Romano *et al.,* 2009). The Ser/Thr kinase mTOR is coordinated by intracellular positioning of lysosomes in response to nutrient availability (Poüs and Codogno, 2011) and exists in the form of two complexes, one of which (mTORC1) is sensitive to rapamycin (Loewith *et al.,* 2002). Activation of mTORC1 correlates with its presence on peripheral lysosomes, which are physically close to the upstream signalling modules (Korolchuk *et al.,* 2011). It remains to be determined whether MT-induced lysosome scattering correlates with active mTOR associated to lysosomes positioned at cell edges, which are the preferential sites for trypomastigote invasion (Mortara, 1991).

Metacyclic trypomastigotes and TCT engage diverse molecules to interact with and invade target cells. Among the surface molecules implicated in invasion are members of the gp85/trans-sialidase superfamily, gp82 and Tc85-11, which are expressed in MT and TCT, respectively, and share 54% sequence identity and have similar 3D structures (Yoshida *et al.,* 2006; Marroquin-Quelopana *et al.,* 2004; Alves and Colli, 2007; Cortez *et al.,* 2012). Gp82 and Tc85-11 may differentially interact with host cells, provided that their cell adhesion sites are distinct; those of gp82 are localized in the C-terminal domain (Cortez *et al.,* 2012), whereas the functionally equivalent sites in Tc85-11 are present in the N-terminal domain (Marroquin-Quelopana *et al.,* 2004). Metacyclic stage gp82 is an adhesin that triggers host cell Ca^{2+} signal (Ruiz *et al.,* 1998), actin cytoskeleton disorganization (Cortez *et al.,* 2006), lysosome scattering and exocytosis (Martins *et al.,* 2011). There is no information whether Tc85-11 has such properties. The sole TCT component reported to trigger Ca^{2+} response and microfilament rearrangement in host cells is a soluble factor of unknown structure (Rodríguez *et al.,* 1995). Using human epithelial HeLa cells, we investigated in this study the importance of lysosome biogenesis/scattering in MT and TCT invasion. We have found that gp82-mediated MT invasion is associated with lysosome biogenesis, whereas TCT entry is predominantly lysosome-independent.

Results

Lysosome biogenesis/scattering and exocytosis induced by short-term nutrient deprivation increase host cell invasion by Trypanosoma cruzi *metacyclic trypomastigotes but inhibit tissue culture trypomastigotes entry*

Metacyclic trypomastigotes invasion of HeLa cells has been shown to be more efficient in medium briefly deprived from nutrients than in full nutrient medium (Martins *et al.,* 2011; Maeda *et al.,* 2012). Here, we compared the ability of MT and TCT to enter HeLa cells in full nutrient D10 medium and in nutrient-free PBS^{++}. We ascertained that HeLa cells remain healthy after 1 h incubation in PBS^{++} by performing assays using fluorescent Annexin-V and SYTOX staining, which detect early stage apoptotic cells and necrotic cells respectively. Flow cytometry analysis showed that cells incubated for 1 h in PBS^{++} preserved their integrity, displaying high cell viability (96.1%), similar to control cells in full nutrient medium (Fig. S1). The viability of cells treated for 4 h with 3 μM staurosporine, which induces apoptosis and necrosis, decreased extensively (data not shown). For invasion assays, MT and TCT were incubated for 1 h with HeLa cells in D10 or PBS^{++} and the number of intracellular parasites was counted. Metacyclic forms were significantly more invasive in PBS^{++} than in D10, whereas TCT invasiveness decreased in PBS^{++} (Fig. 1A). HeLa cells incubated for 1 h in PBS^{++} exhibited lysosomes scattered towards the cell periphery, in contrast to lysosome accumulation at the perinuclear region in cells incubated in D10 (Fig. 1B), as visualized by confocal immunofluorescence using anti-LAMP2 antibody. Lysosome scattering in PBS^{++} was associated with actin cytoskeleton disorganization (Fig. 1C) and resulted in increased exocytosis (Fig. 1D). To quantify lysosomes located at the perinuclear region, a computational algorithm was used. Perinuclear lysosomes, defined as LAMP2-positive voxels of 0.5–1.0 μm in diameter, were identified and counted by software analysis in an expanded region defined by extrapolating the fluorescence signal of the

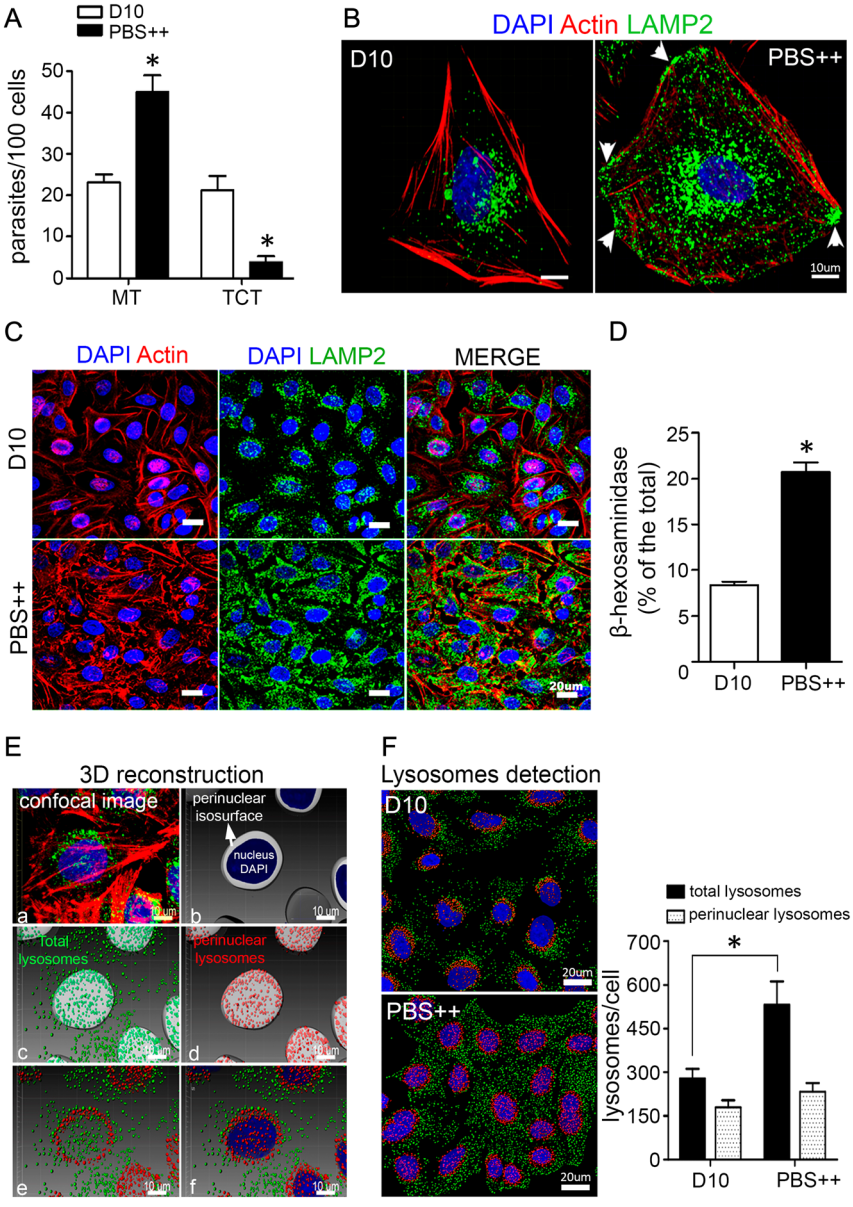

Fig. 1. Lysosome biogenesis/scattering and exocytosis induced by short-term nutrient deprivation increase host cell susceptibility to *T. cruzi* MT and resistance to TCT.
A. Parasites were incubated for 1 h with Hela cells in D10 or in PBS^{++}, and the number of intracellular parasites was counted. Values are the means ± SD of four independent assays performed in duplicate. The difference between D10 and PBS^{++} was significant (*$P < 0.001$).
B,C. Hela cells were incubated for 1 h in D10 or in PBS^{++} and then processed for confocal fluorescence analysis using anti-LAMP2 antibody, Alexa Fluor 488-conjugated anti-mouse IgG (green), phalloidin-TRITC (red) for actin visualization and DAPI (blue) for DNA, with 60× objective. Note in (B) the lysosome scattering and LAMP2 accumulation (arrowhead) at the periphery of cells incubated in PBS^{++}. Scale bar = 10 μm. In (C) the actin cytoskeleton disorganization is seen. Scale bar = 20 μm.
D. Semi-confluent HeLa cell monolayers were incubated in D10 or in PBS^{++}. After 1 h, the supernatants were collected and the release of β-hexosaminidase was measured. Exocytosis was expressed as % of total β-hexosaminidase (supernatant + cell extract). Values are the means ± SD of five independent assays performed in triplicate. The difference between D10 and PBS^{++} was significant (*$P < 0.0001$).
E. Confocal images of LAMP2 immunofluorescence and DAPI staining (a) were processed by Imaris software to construct isosurfaces by extrapolating the DAPI signal to define a perinuclear region where lysosomes can be differentially counted (b). After counting total lysosomes by Imaris isospots function (c), the lysosomes contained within perinuclear region was quantified (d). The isospots corresponding to total and perinuclear lysosomes were depicted in green and red, respectively, (e) and also merged with DAPI signal to ratify the robustness of the method (f). More details in Methods section.
F. From confocal images of HeLa cells cultivated for 1 h in D10 or PBS^{++}, the algorithm-based identification of total lysosomes (green) and perinuclear lysosomes (red) allowed quantification of lysosomes per cell. Values in bar graph correspond to mean ± SD of five different microscopic fields (≥ 120 cells) processed for algorithm-based lysosome countings. The difference in total lysosome numbers presented by cells cultivated in D10 and PBS^{++} was significant (*$P < 0.005$).

nuclear probe 4,6-diamidino-2-phenylindole (DAPI) (Fig. 1E). LAMP2-positive voxels, counted in the area equivalent to the whole cell, corresponded to total lysosomes. These voxels, represented as spots corresponding to perinuclear and total lysosomes, correlated with the immunofluorescence pattern (Fig. 1F). As compared with cells incubated in D10, the total number of lysosomes increased significantly in PBS^{++}, whereas no significant difference was observed in the number of perinuclear lysosomes (Fig. 1F), indicating that lysosome scattering is connected to biogenesis.

Sucrose-induced production of lysosome-like vesicles increases host cell susceptibility to metacyclic trypomastigotes invasion but inhibits tissue culture trypomastigotes internalization

To further assess the influence of lysosome availability in MT and TCT invasion, the production of lysosome-like vesicles (sucrosomes) was induced by growing HeLa cells in D10 for 36 h, in the absence or in the presence of 0.1 M sucrose, an optimal concentration that stimulates increase in lysosome amounts without causing osmotic stress (Karageorgos *et al.,* 1997). Growth of HeLa cells in the presence of sucrose resulted in a numerical increase in large, phase-bright, sucrosomes (Fig. 2A). Treatment with sucrose did not affect cell viability. A high percentage of sucrose-treated cells (86.9%) remained viable, as evidenced by fluorescent Annexin V and SYTOX staining (Fig. S1). Untreated and sucrose-treated HeLa cells were incubated with MT or TCT for 1 h, and the number of intracellular parasites was counted. Cells pretreated with sucrose were significantly more susceptible to MT infection and more resistant to TCT invasion (Fig. 2B). To confirm that sucrosomes were positive for lysosome markers, confocal microscopy images of untreated and sucrose-treated cells, processed for immunofluorescence using anti-LAMP2 antibody, were analysed. LAMP2-positive sucrosomes occupying most of the cytoplasm were visualized in sucrose-treated cells (Fig. 2C). Quantification of lysosomes confirmed significantly higher numbers in cells pretreated with sucrose as compared

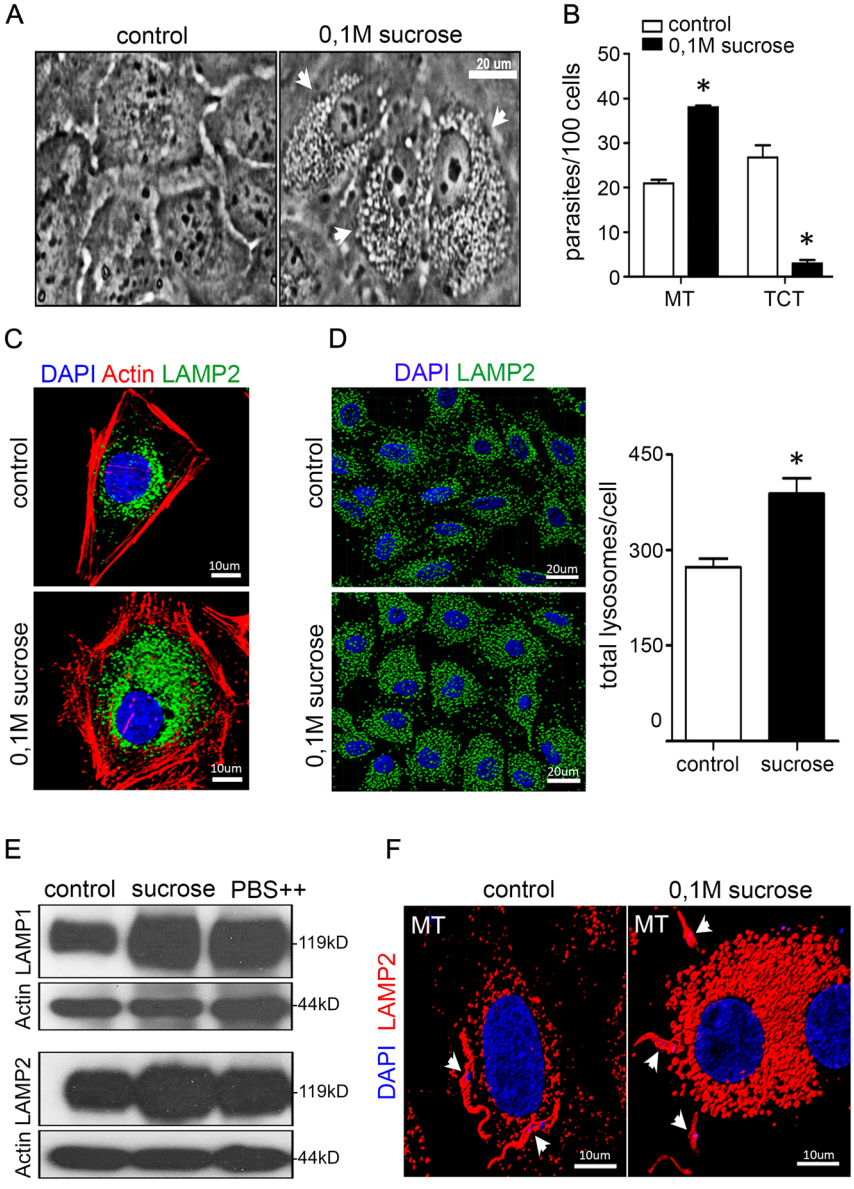

Fig. 2. Sucrose-induced production of host cell lysosome-like vesicles increases MT invasion but inhibits TCT internalization.
A. HeLa cells were grown in the presence or absence of 0.1 M sucrose for 36 h in D10, and then the images were acquired using phase contrast microscope, under 40× objective. Scale bar = 20 μm. Arrows point to large, phase-bright, swollen lysosomes in cells treated with sucrose.
B. Untreated and sucrose-treated cells were incubated with MT or TCT for 1 h in D10, and the number of internalized parasite was counted. Values correspond to means ± SD of five independent experiments performed in duplicate. The difference between untreated control and sucrose-treated cells was significant for MT (*$P < 0.0001$).
C. Untreated and sucrose-treated cells were incubated for 1 h in D10 and processed for confocal fluorescence analysis (actin in red, LAMP2 in green and nucleus is blue) under 60× objective. Scale bar = 10 μm.
D. For lysosome quantification, the 3D construction of images was used (60× objective). Scale bar = 20 μm. Values in the bar graph are the means ± SD of five microscopic fields (≥ 70 cells). The difference between total lysosomes in untreated and sucrose-treated cells was significant (*$P < 0.05$).
E. Western blots of lysates of HeLa cells, untreated or treated with sucrose and then incubated for 1 h in D10, were probed for LAMP1, LAMP2 and β-actin.
F. HeLa cells pretreated or not with sucrose were incubated for 1 h with MT and processed for confocal immunofluorescence using anti-LAMP2 antibody and DAPI for visualization of lysosomes (red) and nucleus (blue) respectively. Scale bar = 10 μm.

with untreated controls (Fig. 2D). In Western blots, increased levels of lysosomal membrane proteins LAMP1 and LAMP2 were detected in sucrose-treated cells, similar to those induced by PBS^{++} (Fig. 2E). Most invading or recently internalized MT were LAMP2-positive (Fig. 2F).

Interaction of host cells with metacyclic trypomastigotes, but not tissue culture trypomastigotes, induces mammalian target of rapamycin dephosphorylation, transcription factor EB translocation to the nucleus and lysosome biogenesis

The transcription factor EB (TFEB) is a regulator of lysosomal biogenesis that, upon sucrose supplementation to the culture medium, was found to translocate from the cytoplasm to the nucleus (Sardiello *et al.,* 2009). Transcription factor EB interacts with and is phosphorylated by mTORC1 at the lysosomal surface and translocates to the nucleus when it is activated by inhibition of mTOR (Settembre *et al.,* 2012; Settembre and Medina, 2015). We examined the ability of MT and TCT to induce mTOR dephosphorylation and nuclear TFEB translocation. HeLa cells were incubated for 30 min with MT or TCT and then processed for Western blot analysis using anti-phosphorylated mTOR antibodies and appropriate loading controls. The phosphorylation levels of mTOR were reduced in cells incubated with MT, whereas no such alteration was observed in cells that interacted with TCT (Fig. 3A). As the eukaryotic translation initiation factor 4E binding protein (4E-BP1) is the downstream target of mTOR (Gingras *et al.,* 2004), we also examined the

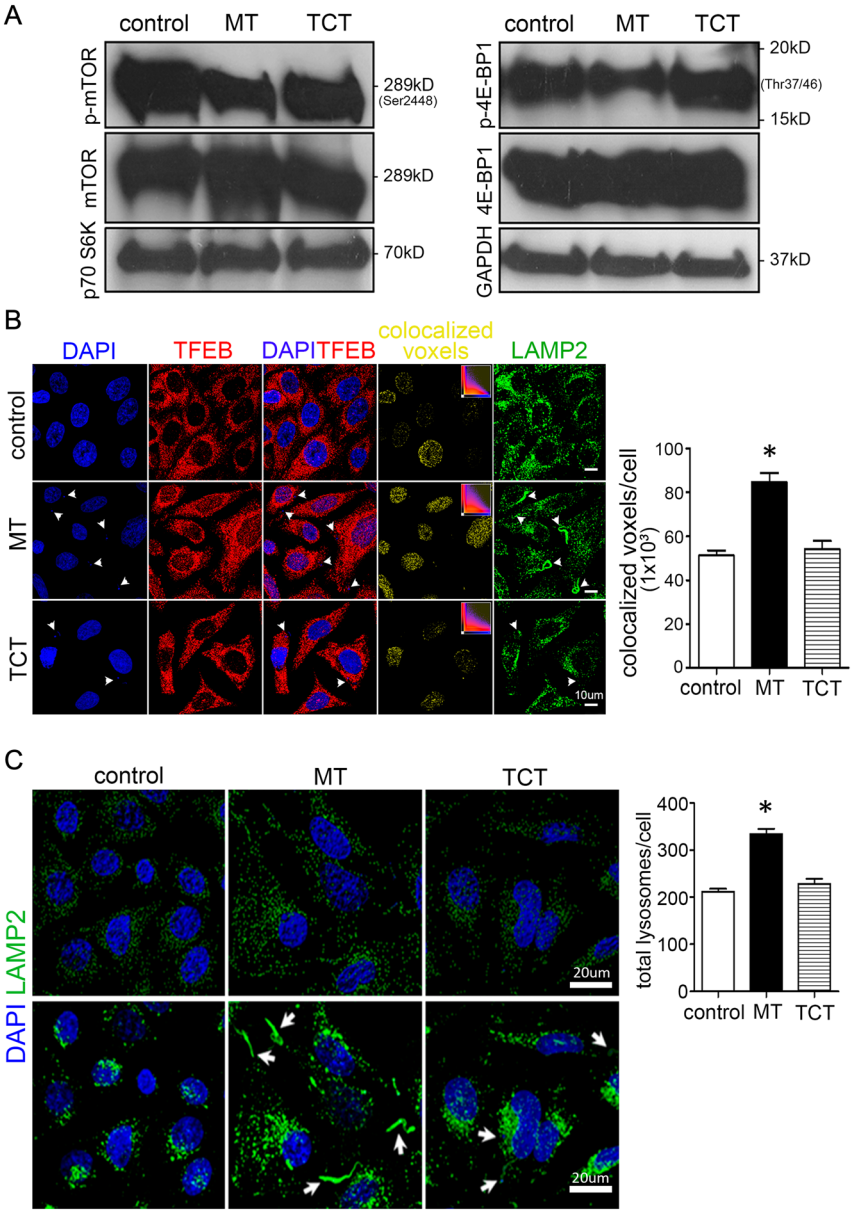

Fig. 3. Lysosome biogenesis and nuclear translocation of TFEB are induced in host cells by *T. cruzi* MT but not by TCT.
A. HeLa cells were incubated for 30 min with MT or TCT, and the cellular lysates were analysed by Western blot, using antibodies to mTOR, phosphorylated mTOR, p70S6K, 4E-BP1, phosphorylated 4E-BP1 and GPDH. Note a decreased phosphorylation level of mTOR and 4E-BP1 upon interaction with MT but not with TCT.
B. HeLa cells were incubated for 30 min with MT or TCT and then processed for confocal immunofluorescence to visualized lysosomes (green), TFEB (red) and nucleus (blue). Colocalized DAPI/TFEB voxels (yellow) are depicted in the fourth column, where the inset shows the histogram of DAPI (blue, *Y*-axis) and TFEB (red, *X*-axis) fluorescence intensity. Parasites are indicated by arrowheads. Note that MT, but not TCT, induced TFEB translocation to the nucleus. Imaris software was used to evaluate the nuclear translocation of TFEB, based on DAPI/TFEB colocalization. The graph shows the means ± SD of 10 microscopic fields (≥ 300 cells) (60× objective). Scale bar = 10 μm. The colocalized DAPI/TFEB voxels were significantly higher in cells upon interaction with MT ($*P < 0.001$).
C. HeLa cells were incubated for 30 min with MT or TCT and then processed for confocal immunofluorescence for quantification of lysosomes (green). The 3D construction of confocal images (upper panel) was used for lysosome quantification. Values in the graph are the means ± SD of 10 microscopic fields (≥ 300 cells) (60× objective) Scale bar = 20 μm. Interaction with MT, but not with TCT, resulted in significantly increased number of total lysosomes ($*P < 0.0001$). Note in the lower panel intense LAMP2 staining of MT but not of TCT.

phosphorylation levels of this factor in cells incubated with MT or TCT. Compatible with MT-induced mTOR inhibition, the 4E-BP1 phosphorylation levels decreased upon incubation of HeLa cells with MT but not with TCT (Fig. 3A). Analysis of HeLa cells processed for immunofluorescence to detect TFEB revealed an extensive nuclear TFEB translocation upon 30 min incubation with MT but not with TCT (Fig. 3B). Using Imaris software (Bitplane, Belfast, UK), we confirmed the MT-induced increase in nuclear TFEB localization by quantifying colocalized DAPI/TFEB (Fig. 3B, graph). To confirm our prediction that MT, but not TCT, induced lysosome biogenesis, parasites were incubated for 30 min with HeLa cells and then processed for confocal immunofluorescence analysis, using anti-LAMP2 antibody. Lysosome quantification using the 3D construction of confocal images (Fig. 3C, upper panel) indicated that MT, but not TCT, induced a significant increase in the lysosome numbers (Fig. 3C, graph). Most MT were strongly stained with lysosome marker LAMP2, whereas very few TCT were LAMP2-positive (Fig. 3C, lower panel).

Host cell susceptibility to metacyclic trypomastigotes, but not to tissure culture trypomastigotes, is associated with mammalian target of rapamycin and TFEB signalling pathways

First, we checked the association of parasites with mTORC1 present on lysosomes and then examined the effect of mTORC1 inhibitor rapamycin on lysosome distribution and parasite invasion. HeLa cells were incubated with MT or TCT for 30 min, and processed for immunofluorescence analysis using antibodies directed to LAMP2 or mTOR. As shown in Fig. 4A, colocalized LAMP2/mTOR was detected surrounding MT, whereas a

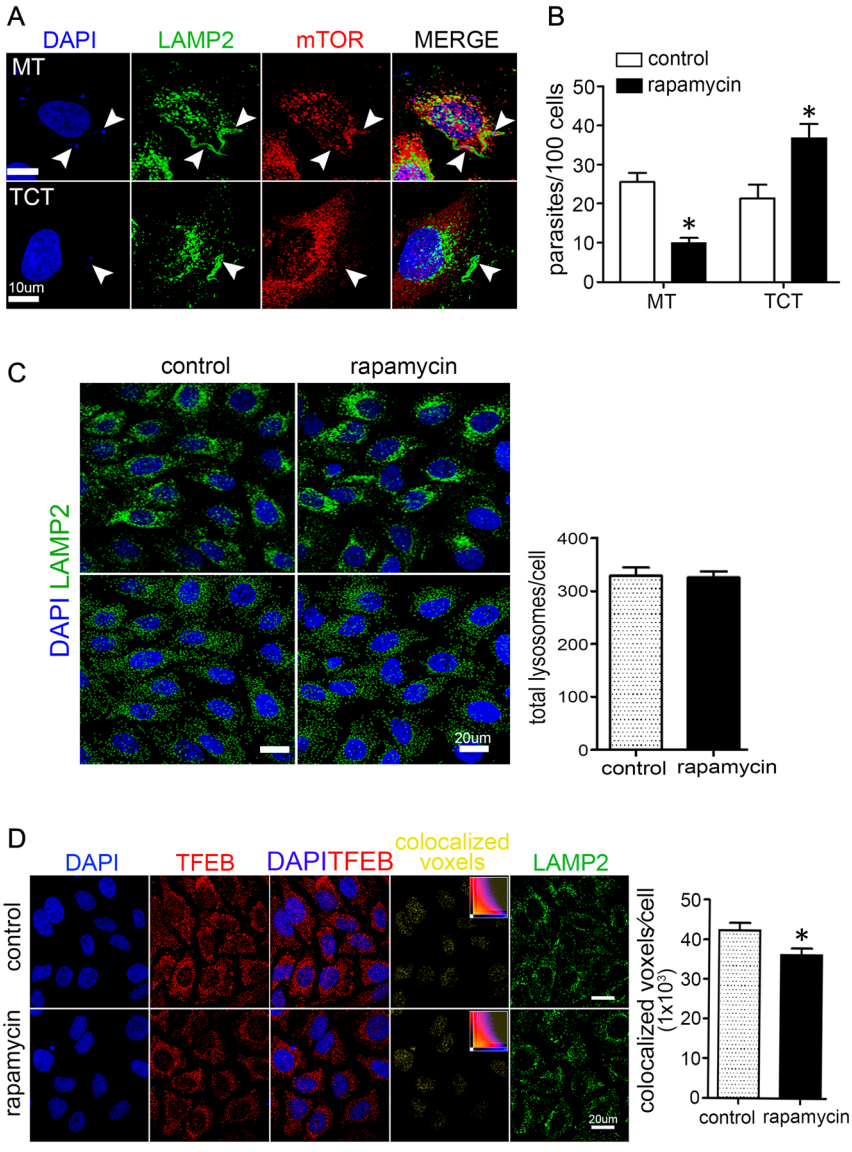

Fig. 4. Inhibition of mTORC1 by rapamycin decreases *T. cruzi* MT invasion and stimulates TCT entry into host cells.
A. HeLa cells were incubated for 30 min with MT or TCT and processed for immunofluorescence analysis, to check their association with LAMP2 (green) and/or mTOR (red). Scale bar = 10 μm. Parasites are indicated by arrowheads. MT surrounded by LAMP2, and mTOR were visualized at the periphery of cells with scattered lysosomes, whereas a few TCT were LAMP2-positive but negative for mTOR.
B. HeLa cells were treated for 30 min with 100 nM rapamycin. After removal of the drug, the cells were incubated for 1 h with MT or TCT, and the number of intracellular parasites was counted. Values correspond to means ± SD of four independent assays performed in duplicate. Rapamycin significantly inhibited MT invasion ($^*P < 0.005$) and stimulated TCT internalization ($^*P < 0.05$).
C. Rapamycin-treated and untreated cells were processed for immunofluorescence to quantify lysosomes (60× objective). Note in the upper panel the rapamycin-induced perinuclear accumulation of lysosomes. Quantification of lysosomes using the 3D construction of confocal images (lower panel) did not reveal any difference in lysosome numbers in rapamycin-treated cells as compared with untreated controls.
D. Rapamycin-treated and untreated Hela cells were processed for confocal immunofluorescence for detection of lysosomes (green), TFEB (red) and nucleus (blue). Colocalized DAPI/TFEB voxels were quantified using Imaris software. Values in the bar graph are the means ± SD of six microscopic fields (≥ 150 cells). There was a small, but significant, difference between rapamycin-treated and untreated cells ($^*P < 0.05$). Scale bar = 20 μm.

few TCT that acquired lysosome marker was negative for mTOR. The possibility that MT reacted with anti-LAMP2 or anti-mTOR antibodies was ruled out. Metacyclic trypomastigotes reacted with monoclonal antibody directed to the surface molecule gp82 but were not recognized by antibodies directed to LAMP2, mTOR or phosphorylated mTOR (Fig. S2). To check the effect of rapamycin, HeLa cells were treated for 30 min with 100 nM of the drug and, after its removal, were incubated for 1 h with MT or TCT, along with untreated controls. Rapamycin treatment, which did not have deleterious effect on HeLa cells, as checked by flow cytometry analysis of cells after fluorescent Annexin V and SYTOX staining (Fig. S1), inhibited MT invasion and stimulated TCT entry (Fig. 4B). Immunofluorescence analysis of rapamycin-treated cells revealed that lysosomes accumulated in the perinuclear region (Fig. 4C, upper panel). Lysosome quantification using the 3D construction of confocal images (Fig. 4C, lower panel) indicated that the lysosome numbers were comparable in untreated and rapamycin-treated cells (Fig. 4C, graph). Transcription factor EB localization was predominantly cytoplasmic in both cells (Fig. 4D). A slight but significant decrease in colocalized DAPI/TFEB was detected in rapamycin-treated cells (Fig. 4D, graph). This may explain the rapamycin-induced decrease in lysosome exocytosis shown by Martins *et al.* (2011).

Metacyclic trypomastigotes surface molecule gp82 induces LAMP2/mammalian target of rampamycin accumulation at cell edges, mammalian target of rampamycin dephosphorylation, nuclear transcription factor EB translocation and lysosome biogenesis/scattering

As MT invasion is mediated by the surface molecule gp82, we investigated whether gp82 binding to HeLa cells triggered the events observed upon interaction with parasites. HeLa cells were incubated for 30 min with 20 $\mu g\ ml^{-1}$ recombinant protein rGP82, containing the full length gp82 sequence fused to gluthatione S-transferase (GST), or with GST as a control, and the cells were processed for immunofluorescence and Western blot analyses. Evaluation of confocal images, using Imaris software, revealed that rGP82, but not GST, induced LAMP2/mTOR colocalization at the cell edges (Fig. 5A). In Western blots, decreased phoshorylation levels of mTOR and 4E-BP1 were detected in cells that interacted with rGP82 but not with GST (Fig. 5B).

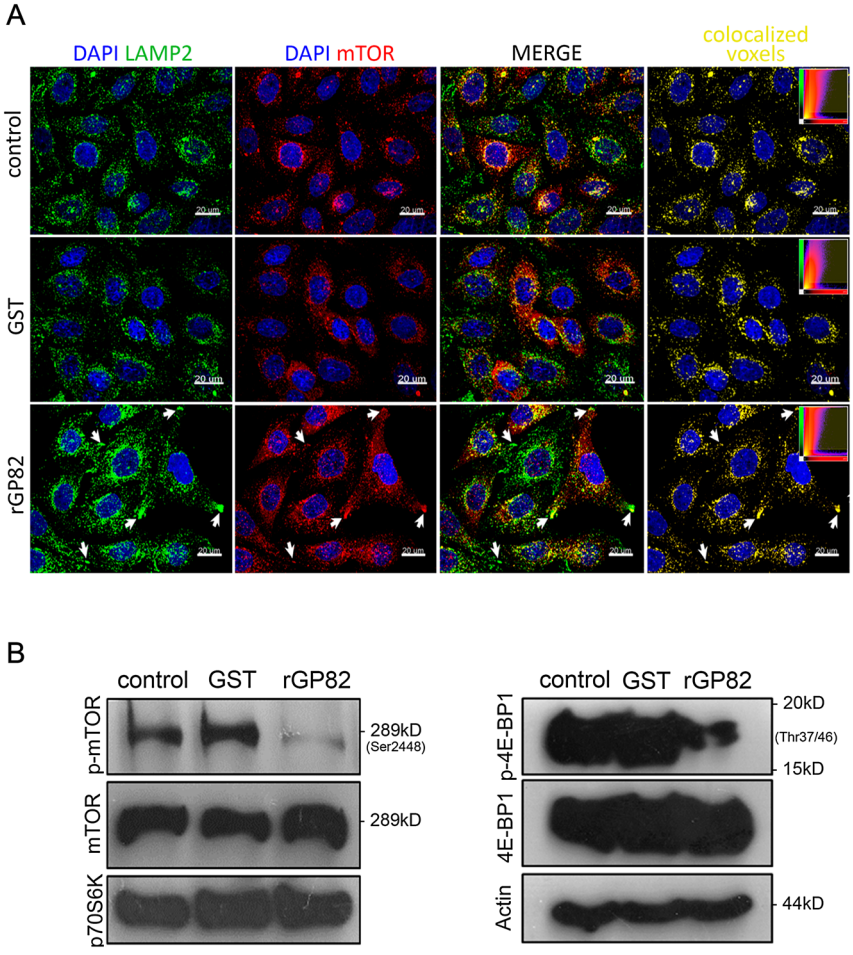

Fig. 5. *Trypanosoma cruzi* MT surface molecule gp82 induces mTOR dephosphrylation and LAMP2/mTOR accumulation at cell edges.
A. HeLa cells were incubated for 30 min with 20 $\mu g\ ml^{-1}$ rGP82 or GST and processed for detection of LAMP2 (green) and mTOR (red). LAMP2/mTOR colocalization was evaluated using Imaris software. Note that rGP82, but not GST, induced LAMP2/mTOR colocalization at the cell edges (arrows). Scale bar: 20 μm.
B. Western blots of extracts of HeLa incubated with rGP82 or GST were probed for mTOR, phosphorylated mTOR, p70S6K, 4E-BP1, phosphorylated 4E-BP1 and β-actin. Note the decreased phosphorylation levels of mTOR and 4E-BP1 induced by rGP82 but not by GST.

Immunofluorescence analysis for detection of TFEB and LAMP-2 showed that rGP82 induced TFEB translocation to the nucleus, whereas GST had no effect (Fig. 6A), and increased nuclear localization of TFEB was confirmed by quantification of colocalized DAPI/TFEB (Fig. 6A, graph). Lysosome biogenesis induced by rGP82, but not by GST, was confirmed by lysosome quantification (Fig. 6B), as well as by increased levels of LAMP1 and LAMP2 detected in Western blots (Fig. 6C). We also checked the association of raptor/lysosomes. Raptor, the regulatory associated protein of mTOR, interacts with mTORC1 substrates S6K and 4E-BP1 and is an essential scaffold for the mTOR-catalysed phosphorylation of 4E-BP1 (Hara *et al.,* 2002). Immunofluorescence analysis of cells revealed an extensive LAMP2/Raptor association, particularly in rGP82-stimulated cells (Fig. S3).

Discussion

Our study, using MT and TCT as counterparts of insect-borne metacyclic forms and trypomastigotes, which circulate in the mammalian bloodstream, has indicated that these *T. cruzi* forms enter target cells through distinct mechanisms. MT invasion is mainly associated with host cell lysosome biogenesis/scattering, whereas TCT entry is predominantly lysosome-independent. Conditions that stimulated lysosome biogenesis/scattering, such as short time incubation in nutrient-deprived medium or treatment with sucrose, had opposite effects on invasion by MT and TCT: the susceptibility to MT increased and to TCT diminished. The relevance of lysosome in MT but not in TCT invasion was further demonstrated by experiments in which the host cells were treated with rapamaycin. This drug promoted lysosome accumulation at the perinuclear

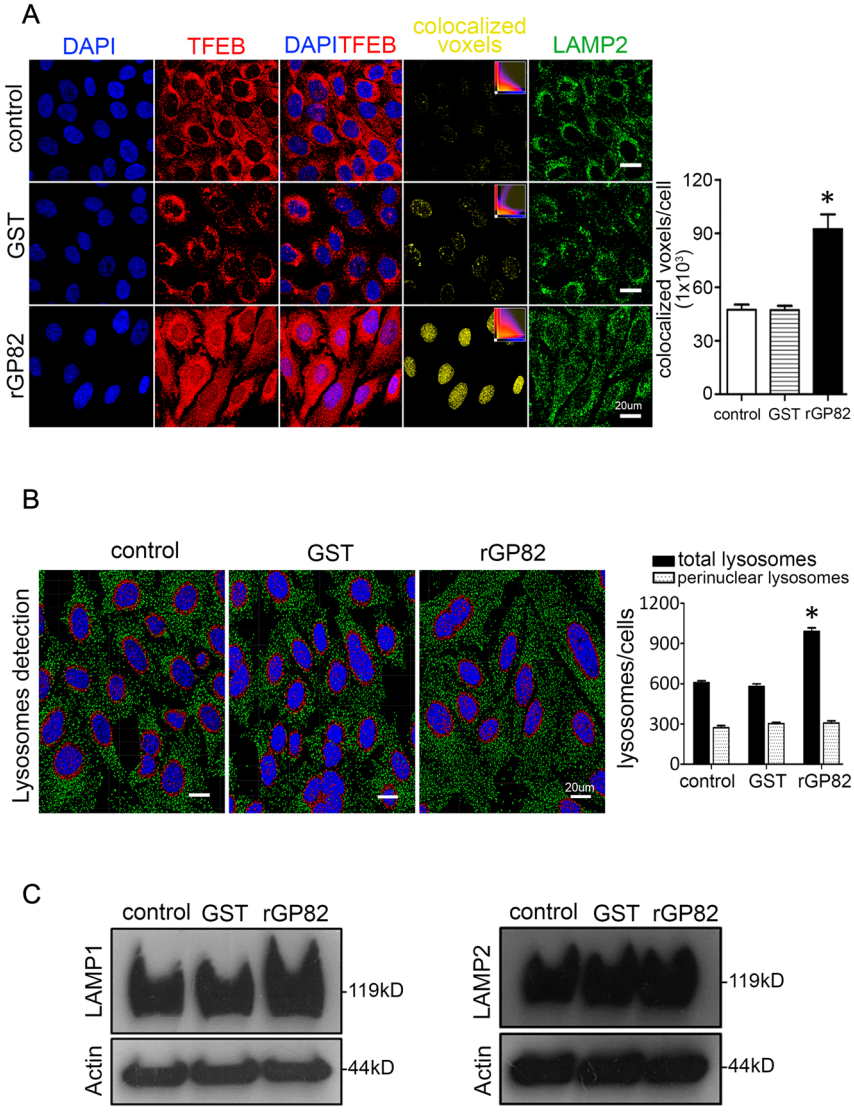

Fig. 6. Nuclear translocation of TFEB and lysosome biogenesis/scattering is induced by *T. cruzi* MT surface molecule gp82.
A. HeLa cells were incubated for 30 min with 20 μg ml^{-1} recombinant gp82 (rGP82), which is fused to GST, or with GST, and then processed for confocal immunofluorescence for detection of TFEB (red), LAMP2 (green) and nucleus (blue). Scale bar = 20 μm. Note that rGP82, but not GST, induced TFEB nuclear translocation and lysosome scattering. Colocalized DAPI/TFEB voxels were quantified using Imaris software. Values in the bar graph are the means ± SD of 10 microscopic fields (≥ 300 cells). Colocalized voxels increased significantly in HeLa cells upon interaction with rGP82 (*$P < 0.0001$) but not with GST.
B. HeLa cells incubated for 30 min with 20 μg ml^{-1} recombinant rGP82 or GST were processed for lysosome quantification. Shown are the representative images of cells used for lysosome quantification by 3D construction of confocal images, exhibiting total (green) and perinuclear (red) lysosomes, in addition to nucleus (blue). Bar: 20 μm. A significant increase in the number of lysosomes, induced by rGP82 (*$P < 0.0001$) but not by GST, is shown in the bar graph.
C. Western blots of extracts of HeLa incubated for 30 min with rGP82 or GST were probed for LAMP1, LAMP2 and β-actin. Note the increase in the intensity of bands corresponding to LAMP1 and LAMP2 in cells incubated with rGP82 but not with GST.

region, leading to increased resistance to MT and higher susceptibility to TCT. The observation that a lysosome-independent mechanism prevails in TCT invasion confirms previous findings by another research group that used a different *T. cruzi* strain and diverse mammalian cell types markers (Woolsey *et al.,* 2003; Woolsey and Burleigh, 2004; Burleigh, 2005). What has been reported is that lysosomes are not required for the TCT invasion process, but they are essential to ensure effective internalization. Initially, TCTs are devoid of lysosomal markers, then the resultant parasite-containing vacuoles gradually acquire lysosome associated membrane protein, the formation of a parasitophorous vacuole with lysosomal properties being essential for preventing TCT from exiting host cells (Woolsey *et al.,* 2003; Andrade and Andrews, 2004; Woolsey and Burleigh, 2004).

Several pieces of evidence have shown that MT, but not TCT, associates with active mTOR at peripheral lysosomes and induces its dephoshorylation, as well as nuclear translocation of TFEB and lysosome biogenesis. Consistent with these findings, MT was internalized within a vacuole with colocalized lysosome marker LAMP2/mTOR. When cells were treated with mTORC1 inhibitor rapamycin, the lysosomes further concentrated in the perinuclear region. As rapamycin enhances lysosomal accumulation of mTOR (Ohsaki *et al.,* 2010), presumably fewer lysosomes associated with active mTOR would be available at the cell periphery upon interaction with MT. On the other hand, TCT invasion, which relies on the formation of a tightly associated host cell plasma membrane-derived vacuole (Woolsey *et al.,* 2003), would be favoured by rapamycin-triggered inward recoiling of lysosomes. Of note was that the recombinant protein based on gp82, the main mediator of MT invasion, induced mTOR dephosphorylation, TFEB translocation to the nucleus, lysosome biogenesis/scattering and mTOR/LAMP2 colocalization at the cell edges, which are the preferential invasion sites used by the parasites (Mortara, 1991).

Disruption of the target cell actin cytoskeleton, an event common to MT and TCT invasion (Rodríguez *et al.,* 1995; Cortez *et al.,* 2006), was suggested to play a role in *T. cruzi* invasion, by facilitating lysosome access to the invasion site (Rodríguez *et al.,* 1995). In the case of MT, the connection between F actin depolymerization and lysosome scattering is compatible with the gp82-mediated invasion. Our previous study with CL strain showed that treatment of host cells with cytochalasin D increased MT invasion to some degree and that MT, as well as the recombinant gp82 protein, triggered the disruption of the actin cytoskeleton architecture (Cortez *et al.,* 2006; Ferreira *et al.,* 2006). We have found that MT invasion increased under short time nutrient deprivation, a condition that induced extensive actin cytoskeleton disruption and lysosome biogenesis/scattering. The increased MT invasion capacity would result from the additive effects triggered by the referred condition and by gp82-mediated invasion process, greatly facilitating parasite entry. On the other hand, as regards TCT, experiments using cytochalasin D demonstrated that disruption of host cell actin microfilaments does not augment the lysosome-dependent entry pathway (Woolsey and Burleigh, 2004).

Based on our results, we envisage a scenario schematically depicted in Fig. 7. By binding to target cells in a gp82-mediated manner, the metacyclic forms induce the mobilization of lysosomes to the cell periphery and are internalized in a vacuole containing mTOR and lysosome marker. Metacyclic trypomastigotes-induced mTOR inactivation and nuclear TFEB translocation promote lysosome biogenesis, thus ensuring the availability of these organelles for fusion with the plasma membrane. As lysosomes accumulate in the perinuclear region in cells pretreated with rapamycin and rapamycin enhances lysosomal accumulation of mTOR, MT invasion is impaired by the diminished availability of mTOR/lysosome at the cell periphery. In contrast, TCT invasion, which is favoured when lysosomes are scarce at the cell periphery, the rapamycin-induced perinuclear lysosome localization contributes to the lysosome-independent TCT internalization. The differences between the mode of invasion of MT and TCT are possibly associated with distinct signalling pathways triggered by these parasite

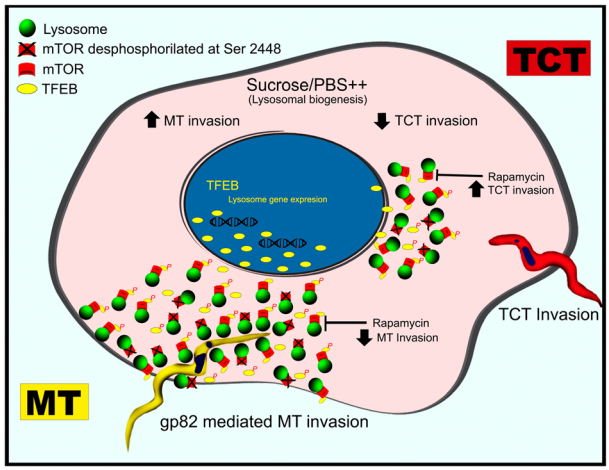

Fig. 7. Schematic representation of host cell invasion by *T. cruzi* MT and TCT. Binding of MT to host cell, mediated by gp82, triggers lysosome mobilization to the cell periphery. Gp82 induces dephosphrylation of mTOR associated with TFEB at the lysosome surface, TFEB translocation to the nucleus and lysosome biogenesis. TCT invasion is predominantly lysosome-independent. Conditions that stimulate lysosome biogenesis and/or scattering, such as short term incubation in nutrient-deprived PBS^{++} solution or treatment with sucrose, increase MT invasion and greatly reduce TCT internalization. Conversely, lysosome retention at the perinuclear region, upon treatment with mTOR inhibitor rapamycin, reduces MT invasion and facilitate TCT internalization.

forms, whose counterparts involved in infection of mammalian hosts interact with different target cells under distinct conditions. When MT from insect vectors reaches the host cells through the skin wound, they may enter fibroblasts, epithelial cells or macrophages, whereas upon oral infection, they invade gastric epithelial cells. Trypomastigotes that circulate in the bloodstream have access to different cell types in diverse organs, such as heart, spleen, liver, and so on, which are inaccessible to MT.

Experimental procedures

Parasites and host cell invasion assay

Trypanosoma cruzi strain CL was maintained alternately in mice and in liver infusion tryptose medium containing 5% fetal bovine serum (FBS). All procedures and experiments conformed with the regulation of the Universidade Federal de São Paulo Ethical Committee for animal experimentation, in accord with Resolution No 196 (10/10/1996) of the National Council of Health, and the study was approved by the Committee (CEP No. 1364/11). To differentiate epimastigotes into metacyclic forms, parasites were grown for one passage in Grace's medium (Invitrogen). Metacyclic forms from cultures at the stationary growth phase were purified by passage through diethylaminoethyl-cellulose column, as described (Teixeira and Yoshida, 1986). Tissue culture trypomastigotes obtained as follows: Vero cells were infected with MT. Starting on day six, the parasites released into the medium were collected. HeLa cells, the human carcinoma-derived epithelial cells, were grown at 37°C in D10 (Dulbecco's minimum essential medium supplemented with 10% FBS, 100 $\mu g\,ml^{-1}$ streptomycin and 100 $U\,ml^{-1}$ penicillin), in a humidified 5% CO_2 atmosphere. Cell invasion assays were performed as detailed elsewhere (Yoshida *et al.,* 1989), by seeding the parasites (moi = 10 for MT and 20 for TCT) onto each well of 24-well plates containing 13-mm-diameter round glass coverslips coated with 1.5×10^5 HeLa cells. After 1 h incubation in full nutrient D10 or in PBS^{++} (PBS containing per litre: 140 mg $CaCl_2$, 400 mg KCl, 100 mg $MgCl_2.6H_2O$, 100 mg $MgSO_4.7H_2O$, 350 mg $NaHCO_3$), the coverslips were washed in PBS, fixed in Bouin solution, stained with Giemsa, and sequentially dehydrated in acetone, a graded series of acetone : xylol (9:1, 7:1, 3:7) and xylol. The number of intracellular parasites was counted in a total of 250 Giemsa-stained cells.

Antibodies

Monoclonal antibodies from Cell Signalling Technology were as follows: anti-LAMP1 (D2D11), anti-mTOR (7C10), anti-phospho specific to mTOR Ser2448 (D9C2), anti-4E-BP1 (53H11), anti-phospho specific to 4E-BP1 Thr-37/46 (236B4), anti-GAPDH (14C10), anti-β-actin (13E5), anti-p70S6K (49D7). Anti-human LAMP2 (H4B4) was from Developmental Studies of the Hybridoma Bank, University of Iowa, and anti-TFEB (ab122910 goat-polyclonal antibody) and anti-raptor (EP539Y) were from Abcam.

Indirect immunofluorescence confocal assays

Coverslips with adherent HeLa cells were incubated for 1 h at 37° C in D10 or in PBS^{++}. After fixation with 4% p-formaldehyde in PBS for 30 min, the cells were treated with 50 mM NH_4Cl in PBS for 30 min and washed in PBS. The cells were then incubated for 1 h at room temperature with mouse anti-human LAMP2 diluted 1:4 (v/v) in a PBS solution containing 0.15% gelatin, 0.1% sodium azide and 1% saponin (PGN-Saponin). After washing in PBS, the coverslips were incubated for 1 h with Alexa Fluor 488-conjugated anti-mouse IgG (Invitrogen), diluted 1:250 in PGN-Saponin containing 100 $ng\,ml^{-1}$ phalloidin-TRITC and 10 $\mu g\,m^{-1}$ DAPI (4′,6′-1-diamino-2-phenylindole dihydrochloride), followed by washes in PBS and subsequent mounting of coverslips in p-phenylenediamine/glycerol. The same immunofluorescence procedure was employed for preparation of samples stained with the following antibodies at the indicated dilutions: anti-mTOR 1:100, anti-TFEB 1:100, anti-raptor 1:100. Confocal images of immunostained samples were acquired in a Leica TCS SP8 laser-scanning microscope (Leica, Germany) using an oil immersion Plan-Apochromat 63× objective (numerical aperture 1.4). The series of images obtained from confocal z-stacks were processed and analysed using Leica LAS AF (Leica, 2012, Germany) and Imaris (Bitplane) software.

Algorithm-based detection and quantification of lysosomes

The series of z-stack images acquired at confocal microscopy were processed by Imaris software (Bitplane) for 3D reconstructions and quantification of lysosomes in x-y-z coordinates. Detection and quantification of lysosomes were performed as follows (Fig. 1E). Confocal images of HeLa cells immunostained with anti-LAMP2 (lysosomes) and stained with DAPI (nucleus) were processed by Imaris software, which allows for building isospots and isosurfaces from fluorescence signal (Real and Mortara, 2012). Isosurfaces were constructed by extrapolating the DAPI signal, corresponding to cell nucleus, in order to define a perinuclear region where lysosomes can be differentially counted. Using a mask tool, all LAMP2 signal outside this nuclear/perinuclear isosurface was suppressed, allowing addition of a new LAMP2 fluorescence channel corresponding exclusively to LAMP2 localized in perinuclear area. After this image processing, we obtained a non-filtered LAMP2 signal (corresponding to all or total lysosomes) and a filtered LAMP2 signal localized in perinuclear region, corresponding to perinuclear lysosomes. Isospots were constructed based on these two classes of LAMP2 signal, which allowed the quantification of total and perinuclear lysosomes per microscopic field. The numbers of total and perinuclear lysosomes were normalized with the number of nuclei detected in each analysed microscopic f3ield.

Analysis of cell viability

Cell viability was assessed by flow cytometry using Annexin V-APC Reagents (BD Biosciences, USA) for detection of external-

ized phosphatidylserine in early stage apoptotic cells and SYTOX® Green Nucleic Acid Stain (ThermoFisher Scientific). Live cells are impermeable to this fluorescent probe, which can penetrate the plasma membrane and bind to DNA only when membrane integrity is breached, as occurs in the later stages of apoptosis or in necrosis. HeLa cells were subjected to different treatments and subsequently harvested, washed with PBS and resuspended in binding buffer (10 mM HEPES, pH 7.4, 140 mM NaCl, 4 mM KCl 0.75 mM $MgCl_2$ x $6H_2O$, 1.5 mM $CaCl_2$) at a concentration of 5×10^5 cells ml^{-1}. The cell suspensions were labelled with annexin V-APC and 8 nM SYTOX® Green according to the manufacturer's instructions. After incubation at room temperature for 30 min, cells were analysed in a BD Accuri flow cytometer (BD Biosciences, USA). The results were processed using FLOWjo 10.0.8 software. A total of 20.000 events were collected per sample. Numbers correspond to the percentage of viable (V), apoptotic (A) and necrotic (N) cells.

Analysis of immunofluorescence colocalization

Confocal images of HeLa cells immunostained with anti-mTOR, anti-LAMP2, anti-TFEB or DAPI were processed for colocalization analysis using the coloc tool of Imaris software. The software allows building additional fluorescent channels corresponding to colocalized voxels adjusted by fluorescent thresholds. LAMP2 fluorescent channel was colocalized with mTOR channel, and TFEB channel was colocalized with DAPI channel. Colocalization was depicted as a new image of colocalized voxels (merged with DAPI channel or not) or as dispersion graphs showing the distribution of voxels in relation to their fluorescence intensities for LAMP2 (green channel, *Y*-axis), mTOR (red channel, *X*- axis), TFEB (red channel, *Y*-axis) and DAPI (blue channel, *X*-axis). Applying the same thresholds for all experimental conditions, the software quantifies the number of colocalized voxels between the channels, which was used comparatively.

Exocytosis assay

Confluent HeLa cells monolayers, grown in 24-well plates in D10 without phenol red, were washed in PBS and incubated in 300 μl D10 or PBS^{++}. After 1 h, the supernatants were collected, the cells were lysed in D10 or PBS^{++} containing 1% NP-40, and 30 μl of 1 M sodium acetate pH 4.0 was added to decrease pH. Samples were centrifuged for 5 min at 13 000 g to collect supernatants, 20 μl aliquots were diluted with 60 μl of citrate buffer and 160 μl of 100 mM 4-nitrophenyl N-acetyl-β-D-glucosaminide (Sigma-Aldrich) were added. After 1 h incubation at 37°C, the reaction was stopped by adding 720 μl of 200 mM sodium borate pH 9.8. Absorbance was measured at 405 nm in ELx800 (Bioteck) plate reader. Exocytosis was expressed as % of total β-hexosaminidase activity (supernatant + cell extract).

Induction of sucrosomes

HeLa cells were plated in 75 cm^2 flasks and grown in D10 to reach confluency. Confluent cells were maintained for 36 h in D10 containing 0.1 M sucrose to induce sucrosome formation, while control cells remained in D10 without sucrose. Untreated and sucrose-treated cells were placed onto 24-well plates containing 13-mm-diameter round glass coverslips (1.5×10^5 cells/well). After overnight growth in D10 without sucrose, the cells were processed for Western blotting, cell invasion assays or immunofluorescence for visualization of lysosomes.

Western blot

HeLa cells were lysed and incubated with TNE buffer (0.1 M Tris–HCl, 0.25 M NaCl and 0.05 M EDTA). The cell lysates were submitted to SDS-PAGE electrophoresis at different gel concentrations, depending on the protein under study: 7% for mTOR, phosphorylated mTOR and p70S6K, 13% 4E-BP1, phosphorylated 4BP-1 and GPDH and 10% for LAMP1, LAMP2 and β-actin. Gels were transferred to nitrocellulose membranes and incubated with antibodies, diluted 1:1000 unless otherwise stated, directed to phosphorylated Ser2448 of mTOR, LAMP1, 4E-BP1, phosphorylated Thr-37 and Thr-46 of 4E-BP1, GAPDH, p70S6K, LAMP2 diluted 1:100 and β-actin diluted 1:2000. Membranes were revealed by chemoluminescence using Immobilon Western kit (WBKLSO500, Millipore Corporation).

Statistical analysis

Significance levels were determined from experimental data and calculated using Student *t*-test, implemented in GraphPad Prism5 programme.

Acknowledgements

This work was supported by Fundação de Amparo à Pesquisa do Estado de São Paulo (FAPESP) (Grant 11/51475-3) and Conselho Nacional de Desenvolvimento Científico e Tecnológico (CNPq) (Grant 300578/2010-5). We thank Dr Helena Bonciani Nader for access to INFAR/UNIFESP Confocal and Flow Cytometry Facility, Dr Renato Arruda Mortara for access to confocal microscope at Biomedical Research Building/UNIFESP and Imaris software.

Conflict of interest

We declare that we do not have any potential sources of conflict of interest.

References

Alves, M.J.M., and Colli, W. (2007) *Trypanosoma cruzi*: adhesion to the host cell and intracellular survival. *IUBMB Life* **59**: 274–279.

Andrade, L.O., and Andrews, N.W. (2004) Lysosomal fusion is essential for the retention of *Trypanosoma cruzi* inside host cells. *J Exp Med* **200**: 1135–1143.

Burleigh, B.A. (2005) Host cell signaling and *Trypanosoma cruzi* invasion: do all roads lead to lysosomes? *Sci STKE* **2005**: pe36.

Cortez, M., Atayde, V., and Yoshida, N. (2006) Host cell invasion mediated by *Trypanosoma cruzi* surface molecule gp82 is associated with F-actin disassembly and is inhibited by enteroinvasive *Escherichia coli*. *Microbes Infect* **8**: 1502–1512.

Cortez, C., Yoshida, N., Bahia, D., and Sobreira, T.J.P. (2012) Structural basis of the interaction of a *Trypanosoma cruzi* surface molecule implicated in oral infection with host cells and gastric mucin. *PLoS One* **7**: e42153.

Deretic, V., Singh, S., Master, S., Harris, J., Roberts, E., Kyei, G., *et al.* (2006) *Mycobacterium tuberculosis* inhibition of phagolysosome biogenesis and autophagy as a host defence mechanism. *Cell Microbiol* **8**: 719–727.

Ferreira, D., Cortez, M., Atayde, V.D., and Yoshida, N. (2006) Actin cytoskeleton-dependent and independent host cell invasion by *Trypanosoma cruzi* is mediated by distinct parasite surface molecules. *Infect Immun* **74**: 5522–5528.

Gingras, A.C., Raught, B., and Sonenberg, N. (2004) mTOR signaling to translation. *Curr Top Microbiol Immunol* **279**: 169–197.

Goebel, W., and Kuhn, M. (2000) Bacterial replication in the host cell cytosol. *Curr Opin Microbiol* **3**: 49–53.

Hara, K., Maruki, Y., Long, X., Yoshino, K., Oshiro, N., Hidayat, S., *et al.* (2002) Raptor, a binding partner of target of rapamycin (TOR), mediates TOR action. *Cell* **110**: 177–189.

Karageorgos, L.E., Isaac, E.L., Brooks, D.A., Ravenscroft, E. M., Davey, R., Hopwood, J.J., and Meikle, P.J. (1997) Lysosomal biogenesis in lysosomal storage disorders. *Exp Cell Res* **234**: 85–97.

Korolchuk, V.I., Saiki, S., Lichtenberg, M., Siddiqi, F.H., Roberts, E.A., Imarisio, S., *et al.* (2011) Lysosomal positioning coordinates cellular nutrient responses. *Nat Cell Biol* **13**: 453–460.

Leica (2012) refers to the producer of the software Leica LAS AF.

Loewith, R., Jacinto, E., Wullschleger, S., Lorberg, A., Crespo, J.L., Bonenfant, D., *et al.* (2002) Two TOR complexes, only one of which is rapamycin sensitive, have distinct roles in cell growth control. *Mol Cell* **10**: 457–468.

Maeda, F.Y., Cortez, C., Alves, R.M., and Yoshida, N. (2012) Mammalian cell invasion by closely related *Trypanosoma* species *T. dionisii* and *T. cruzi*. *Acta Trop* **121**: 141–147.

Maeda, F.Y., Cortez, C., and Yoshida, N. (2012) Cell signaling during *Trypanosoma cruzi* invasion. *Front Immunol* **3**: 361.

Marroquin-Quelopana, M., Oyama, S., Aguiar Pertinhez, T., Spisni, A., Aparecida Juliano, M., Juliano, L., *et al.* (2004) Modeling the *Trypanosoma cruzi* Tc85-11 protein and mapping the laminin-binding site. *Biochem Biophys Res Commun* **325**: 612–8.

Martins, R.M., Alves, R.M., Macedo, S., and Yoshida, N. (2011) Starvation and rapamycin differentially regulate host cell lysosome exocytosis and invasion by *Trypanosoma cruzi* metacyclic forms. *Cell Microbiol* **13**: 943–954.

Mortara, R.A. (1991) *Trypanosoma cruzi*: amastigotes and trypomastigotes interact with different structures on the surface of HeLa cells. *Exp Parasitol* **73**: 1–14.

Ohsaki, Y., Suzuki, M., Shinohara, Y., and Fujimoto, T. (2010) Lysosomal accumulation of mTOR is enhanced by rapamycin. *Histochem Cell Biol* **134**: 537–544.

Poüs, C., and Codogno, P. (2011) Lysosome positioning coordinates mTORC1 activity and autophagy. *Nat Cell Biol* **13**: 342–344.

Real, F., and Mortara, R.A. (2012) The diverse and dynamic nature of *Leishmania* parasitophorous vacuoles studied by multidimensional imaging. *PLoS Negl Trop Dis* **6**: e1518.

Rodríguez, A., Rioult, M.G., Ora, A., and Andrews, N.W. (1995) A trypanosome-soluble factor induces IP3 formation, intracellular Ca2+ mobilization and microfilament rearrangement in host cells. *J Cell Biol* **129**: 1263–1273.

Rodriguez, A., Samoff, E., Rioult, M.G., Chung, A., and Andrews, N. (1996) Host cell invasion by trypanosomes requires lysosomes and microtubule/kinesin-mediated transport. *J Cell Biol* **134**: 349–362.

Romano, P.S., Arboit, M.A., Vázquez, C.L., and Colombo, M. I. (2009) The autophagic pathway is a key component in the lysosomal dependent entry of *Trypanosoma cruzi* into the host cell. *Autophagy* **5**: 6–18.

Ruiz, R.C., Favoreto, S., Jr., Dorta, M.L., Oshiro, M.E.M., Ferreira, A.T., Manque, P.M., and Yoshida, N. (1998) Infectivity of *Trypanosoma cruzi* strains is associated with differential expression of surface glycoproteins with differential Ca^{2+} signaling activity. *Biochem J* **330**: 505–511.

Sardiello, M., Palmieri, M., Ronza, A., Medina, D.L., Valenza, M., Gennarino, V.A., *et al.* (2009) A gene network regulating lysosomal biogenesis and function. *Science* **325**: 473–477.

Settembre, C., and Medina, D.L. (2015) TFEB and the CLEAR network. *Methods Cell Biol* **126**: 45–62.

Settembre, C., Zoncu, R., Medina, D.L., Vetrini, F., Erdin, S., Erdin, S., *et al.* (2012) A lysosome-to-nucleus signalling mechanism senses and regulates the lysosome via mTOR and TFEB. *EMBO J* **31**: 1095–1108.

Tardieux, I., Webster, P., Ravesloot, J., Boron, W., Lunn, J.A., Heuser, J.E., and Andrews, N.W. (1992) Lysosome recruitment and fusion are early events required for trypanosome invasion of mammalian cells. *Cell* **71**: 1117–1130.

Teixeira, M.M., and Yoshida, N. (1986) Stage-specific surface antigens of metacyclic trypomastigotes of *Trypanosoma cruzi* identified by monoclonal antibodies. *Mol Biochem Parasitol* **18**: 271–82.

Voth, D.E., and Heinzen, R.A. (2007) Lounging in a lysosome: the intracellular lifestyle of *Coxiella burnetii*. *Cell Microbiol* **9**: 829–840.

Woolsey, A.M., and Burleigh, B.A. (2004) Host cell actin polymerization is required for cellular retention of *Trypanosoma cruzi* and early association with endosomal/lysosomal compartments. *Cell Microbiol* **6**: 829–838.

Woolsey, A.M., Sunwoo, L., Petersen, C.A., Brachmann, S.M., Cantley, L.C., and Burleigh, B.A. (2003) Novel PI 3-kinase-dependent mechanisms of trypanosome invasion and vacuole maturation. *J Cell Sci* **116**: 3611–3622.

Yoshida, N. (2006) Molecular basis of mammalian cell invasion of *Trypanosoma cruzi*. *Anais Acad Braz Ciências* **78**: 87–111.

Yoshida, N., Mortara, R.A., Araguth, M.F., Gonzalez, J.C., and Russo, M. (1989) Metacyclic neutralizing effect of monoclonal antibody 10D8 directed to the 35- and 50-kilodalton surface glycoconjugates of *Trypanosoma cruzi*. *Infect Immun* **57**: 1663–1667.

Supporting information

Additional Supporting Information may be found in the online version of this article at the publisher's web-site:

Fig. S1. Assessment of host cell viability by Annexin-V/SYTOX staining. HeLa cells, treated with 1 M sucrose for 36 h in D10 or with 100 nM rapamycin for 30 min, were incubated for 1 h in full nutrient D10. Untreated cells were incubated for 1 h in D10 or in PBS^{++}. Cells were stained with Annexin V-APC and 8 nM SYTOX® Green and subjected to flow cytometry analysis. Dot plot depicts the results of 20.000 events analyzed using FLOWjo software. Note the high cell viability after different treatments (lower left quadrant). Numbers correspond to the percentage of viable (V), apoptotic (A) and necrotic (N) cells.

Fig. S2. Antibodies directed to mTOR or LAMP2 do not recognize *T. cruzi* MT. Fixed and permeabilized parasites were incubated for 1 h with monoclonal antibody directed to MT-specific glycoprotein gp82 (positive control), or with anti-mTOR, anti phosphortylated mTOR or anti-LAMP2 antibody, followed by Alexa Fluor 488-conjugated anti-mouse IgG (green). DAPI staining shows kinetoplast and nucleus in blue. Parasites were negative for mTOR or LAMP2.

Fig. S3. LAMP2/Raptor colocalization is detectable at the cell periphery upon interaction with rGP82. HeLa cells were incubated for 30 min with rGP82 or GST, at 20 μg/ml, and then processed for detection of LAMP2 (green) and Raptor (red). LAMP2/Raptor colocalization was evaluated using Imaris software. Scale bar = 20 μm.